CrossMark

A Novel Method For Fabricating Cr-Doped Alpha-Al$_2$O$_3$ Nanoparticles: Green Approach To Nanotechnology

Graziele C. da Cunha[1] · Carolina M. Abreu[2] · Janaina A. Peixoto[2] ·
Luciane P. C. Romão[1] · Zélia S. Macedo[2]

Abstract The aim of this work was to produce Cr-doped alpha-alumina nanoparticles using a modified sol–gel method that employs the complexation capacity of natural organic matter (NOM). For this synthesis, the initial pH of the sol was adjusted to 4.0, and final calcination of the xerogel was performed at 1100 °C for 4 h. XRD and FTIR analyses confirmed that the hexagonal α-Al$_2$O$_3$ phase was produced under these conditions. Chromaticity analyses revealed that more intense pink colors were obtained for the samples with higher Cr concentrations. XANES measurements showed that the oxidation state of chromium in the alumina matrix was strongly dependent on the dopant concentration and that it was possible to produce samples free from Cr(VI). The photo- and radioluminescence spectra of the nanoparticles were found to be sensitive to the dopant concentration. All these findings demonstrated that the synthesis procedure using NOM could provide considerable environmental, technological, and economic benefits.

Keywords Natural organic matter · Nanoparticles · Chromium-doped α-alumina · Sol–gel

1 Introduction

The production of inorganic nanopowders has received much attention due to the improved optical, structural, and electronic properties presented by these materials. Furthermore, the development of new eco-friendly synthesis routes meets an increasing social demand for the use of green technologies.

Nanopowders with controlled particle size (smaller than 100 nm) can exhibit unique behavior due to their high specific area, which results in improved surface energy [1–3]. Special attention is given to alumina, the most cost-effective and widely used structural engineering material in the family of advanced ceramics, which has several crystalline phases. Amongst these phases, α-Al$_2$O$_3$ is the most stable and, consequently, is the most studied alumina phase [4]. Since it has excellent thermal and chemical stability, alumina is frequently employed in the energy, oil, and ceramics industries. It is also used as a precursor for various optical and optoelectronic materials [5, 7].

There have been many studies focusing on the luminescence of new materials, and much effort has been dedicated to improving the optical properties of structures that are already known [8, 9]. Aluminum oxide doped with different transition metals, especially chromium, can be highlighted as an excellent luminescence emitter [10, 11]. Doping with Cr also significantly improves the thermoluminescent properties of Al$_2$O$_3$ [12–14]. The ceramics industry is particularly interested in the development of highly stable nanopigments with intense chromaticity that satisfy both technological and environmental demands [15].

The synthesis of inorganic nanomaterials and nanostructures by physical, chemical, and biological methods has been developed in recent decades. The physical and chemical methods can be problematic because they may

✉ Graziele C. da Cunha
  grazy.ufs@gmail.com

1 Chemistry Department, Federal University of Sergipe (UFS), Aracaju, Sergipe 49100-000, Brazil

2 Materials Science and Engineering Department, Federal University of Sergipe (UFS), Aracaju, Sergipe 49100-000, Brazil

be lengthy, expensive, and lead to environmental contamination by the chemical precursors, solvents, or hazardous byproducts [16]. All these drawbacks restrict the use of chemical and physical synthesis routes for large-scale production [17]. As an alternative, eco-friendly biological processes have emerged as a promising option for the production of nanoparticles (NPs) [18].

Biological processes involve the use of natural structures to substitute the reagents traditionally used for the synthesis of NPs [17]. Several different biological resources have been investigated for the bio-production of NPs, including bacteria, fungi, algae, viruses, plants, and plant extracts [19]. A modified sol–gel route, in which natural organic matter (NOM) is used to anchor metal ions, was reported in a previous paper [20] describing the production of non-doped nanoparticles of alpha-alumina.

Despite the evident economic and environmental advantages of these bioprocesses, there remains a lack of investigations concerning their influence on the properties of the nanoparticles produced. It is well known that the synthesis route can be a crucial determinant of the morphology, defects, and other properties of various materials [21]. This work therefore reports a careful investigation of the synthesis parameters used in the production of Cr-doped alumina, as well as the structural, morphological, compositional, and optical properties of the samples produced.

2 Experimental

The NOM-rich water used in the synthesis was collected from a waterfall in Sergipe State, Brazil, and was used without any prior filtering or purification. The water was transported from the waterfall to the laboratory at ambient temperature. The synthesis of non-doped alumina was described previously [20] and a similar procedure was adopted in the present work. The precursors used were $Al_2Cl_3 \cdot 6H_2O$ and $Cr(NO_3)_3 \cdot 9H_2O$, which were dissolved in NOM-rich water, with continuous stirring for 120 min at room temperature, until a gel was formed. This material was then dried at 100 °C, resulting in a porous low density solid (xerogel), which was then homogenized and calcined at different temperatures (800, 900, or 1100 °C) in an open atmosphere muffle furnace in order to remove the organic material and crystallize the desired phase. The tests were conducted using different initial solution pH values (3.0, 4.0, 5.0, 6.0, 7.0, 8.0, or 9.0, adjusted using NH_4OH). The optimum temperature for calcination of the xerogel was also investigated using thermogravimetric (TGA) and differential thermal analysis (DTA) measurements (model SDT 2960 analyzer, TA Instruments). These measurements were performed from room temperature up to 1200 °C, under a 100 mL min^{-1} flow of synthetic air.

X-ray diffraction (XRD) measurements (Rigaku RINT Ultima + 2000/PC) were used for qualitative analysis of the crystalline phases present in the samples. The measurements were performed at room temperature, using Cu Kα radiation, in continuous scan mode in the range from 10° to 80°, with a scanning speed of 1° min^{-1}. The diffractograms were compared to the ICSD (inorganic crystal structure database) cards. Fourier transform infrared (FTIR) spectrometry was used to determine the vibrational modes related to the crystalline phases formed or other molecular species in the samples. For these measurements, the material was mixed with KBr and pelletized. The analyses were performed using a Perkin Elmer instrument in transmission mode, in the range $4000 - 400$ cm^{-1}, with a resolution of 4 cm^{-1}. Semi-quantitative determination of elements with atomic mass ≥4 was performed by X-ray fluorescence spectroscopy (XRF), using an S4 Pioneer X-ray fluorimeter (Bruker). For these measurements, 1 g of the sample was mixed with 9 g of H_3BO_3 and this mixture was pressed into cylindrical pellets. The morphology of the samples was analyzed using a scanning electron microscope equipped with a field emission gun (FEG-SEM, JEOL model JSM-7500F). The size of the particles was estimated using Image J software. For this, around ten images from different regions of the sample were employed. The average size was then calculated using various particles observed in different images (n = ~50).

The valence states of the dopants were determined by X-ray absorption near-edge structure (XANES) measurements at the D08B:XAFS2 beamline of the Brazilian synchrotron light laboratory (LNLS) in Campinas, Brazil. The XANES spectra were obtained at the K-edge of Cr (5989 eV) for the samples and the Cr_2O_3 and $K_2Cr_2O_7$ reference materials (where the valence states of Cr are +3 and +6, respectively).

Diffuse reflectance measurements were performed at room temperature using an integrating sphere. Colorimetric characterization was performed using the OA spectra, following the CIE-L*a*b* 1976 norm, as recommended by the CIE (International Commission on Illumination). The photoluminescence (PL) properties of the samples were determined at room temperature, in both emission and excitation modes. For these measurements, a 300 W xenon lamp coupled to a monochromator was used for excitation. The light output of the samples was monitored with an ocean optics HR 2000 spectrometer.

In order to investigate the feasibility of using the materials as ceramic pigments, leaching tests were performed to determine the degree of immobilization of the chromium ions in the alumina matrix. These tests followed the ABNT-NBR 10.005 norm. The specimens were composite pellets of milled glaze and Al_2O_3:Cr, with glaze to pigment ratios of 9:1, 7:3, and 5:5. The pellets were sintered at 1100 °C for

4 h in a muffle furnace, using a heating rate of 10 °C min⁻¹. The sintered pellets were then ground and sieved, and the resultant powder was stirred for 18 h in a solution containing acetic acid, sodium hydroxide, and distilled water. This suspension was filtered using a 0.45 μm filter and the Cr concentration in the liquid was determined by inductively coupled plasma optical emission spectrometry (ICP-OES). All the tests were repeated at least 3× using different specimens.

3 Results and Discussion

The thermal behavior of the xerogel pre-calcined at 400 °C was investigated in order to identify the best calcination temperature for crystallization of the alumina. Figure 1 presents the TGA/DTA curves for the xerogels produced using 10% Cr and different pH values. The TGA curve for the sample produced with initial pH 3.0 revealed two distinct stages of mass loss from RT up to 800 °C. The first stage occurred before 200 °C, with a mass loss of ~11.1%, and was probably due to dehydration. This hypothesis was supported by the endothermic band observed in the DTA curve (Fig. 1b) and by the peaks observed in the derivative mass loss curve (Fig. 1c). Similar behavior was observed for the samples prepared with initial pH of 4.0, 5.0, 6.0, 7.0, 8.0, and 9.0. For these samples, the mass loss values at 200 °C were 15.6, 14.5, 19.3, 16.0, 16.3, and 16.6%, respectively. In the second stage, there was a small weight loss of approximately 5.2% between 400 and 850 °C, probably due to crystallization of the amorphous phase to form gamma-alumina. This was supported by the exothermic peaks observed in the DTA curve and the derivative mass loss curve (Fig. 1c). For the other samples, this mass loss was observed up to ~800 °C. No exothermic peaks corresponding to the crystallization of gamma-alumina were observed in these DTA curves. This behavior was in agreement with results previously reported in the literature [22, 23].

It can be seen from Fig. 1c–e that similar TGA/DTA curve profiles were obtained for the samples doped with 1 and 10% Cr. In earlier studies, Hafez and El-Fadaly [24] synthesized nanoceramic pigments from Co²⁺-doped alumina–titania and observed that different dopant concentrations did not affect the TGA curve profile, due to the low concentration of dopant. Sivakumar et al. [25] synthesized Cu-doped BaSO₄ nanoparticles using the chemical precipitation method and arrived at the same conclusion.

The X-ray diffraction technique was used to investigate crystallization during the synthesis. Figure 2 presents the XRD patterns of the 2% Cr-doped samples prepared using different initial sol pH values. It can be seen that the sample produced using pH 4.0 consisted of a single phase. This was related to the distribution of Al species as a function

of pH, as well as the complexation capacity of the NOM, which was also dependent on pH.

In the case of aluminum ions present in aqueous solution at pH > 5.0, there is competition between formation of the $Al(OH)_4^-$ complex and the hydrolysis of aluminum. At pH 3.0 and 4.0, almost all the aluminum species are present as Al^{3+}, as can be seen in the Pourbaix diagram of aluminum (as well as from the Eh/pH plot), which provides a graphical representation of the possible stable phases of a metal present at equilibrium. These species were available for complexation by the negatively charged groups present in the NOM. Furthermore, the main functional groups present in the NOM are carboxyls and phenolic hydroxyls. These two groups control the chemical behavior, especially reactions involving cationic exchange, complexation, and chelation, which are strongly pH-dependent [26].

The carboxyl groups are dissociated at pH ≥ 4.0, while phenolic groups are dissociated at pH ≥ 9. At pH > 5, the aluminum ions are negatively charged $[Al(OH)_4^-]$ or in the form of the hydroxide, and consequently are not available for complexation by the NOM, with repulsion between these species and the negatively charged NOM groups.

The deprotonation of the carboxylic groups of the NOM at pH 4.0 enables complexation between these groups and the Al^{3+} ions. It has been reported previously that interaction of aluminum ions with humic substances can occur due to hydrogen bonding, electrostatic attraction, ionic exchange, and chelation [27], with the interaction mechanism being dependent on the pH of the solution. Hence, it can be inferred that the main mechanism responsible for the formation of alpha-alumina using NOM was ionic exchange, because under the conditions of the synthesis, the deprotonated carboxyl groups could interact with Al^{3+} present in the medium, following the proposed mechanism shown in Equations 1 and 2.

$$\text{(1)}$$

$$\text{(2)}$$
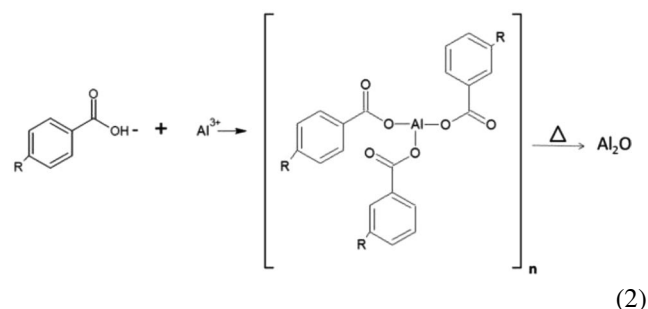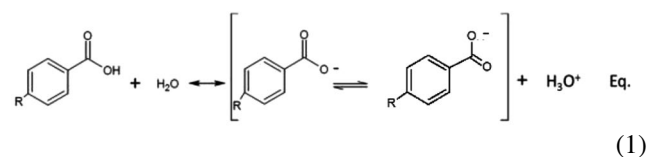
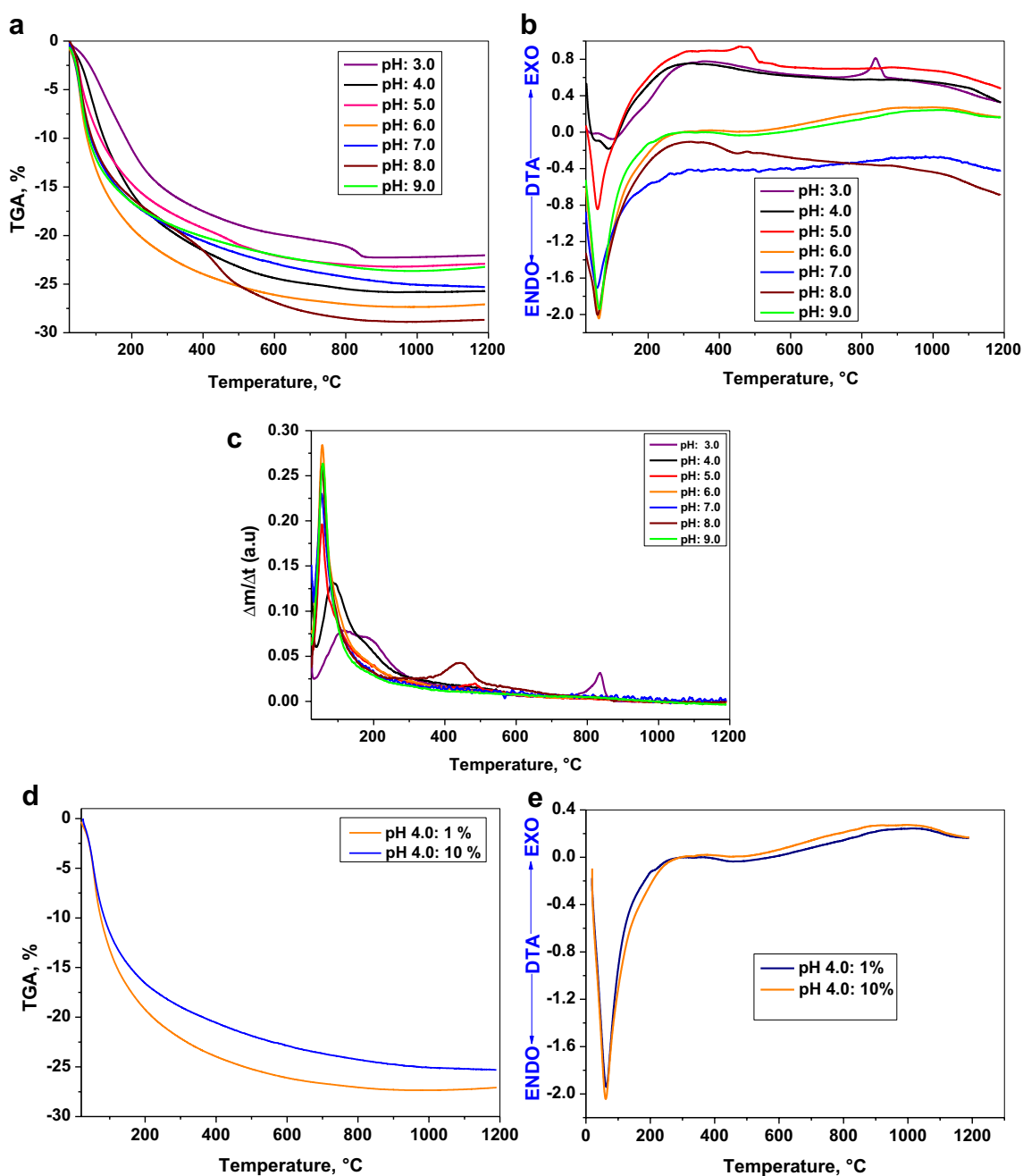The material obtained at pH 7.0 is also shown in Fig. 2. In the presence of the intermediate kappa-alumina

Fig. 1 **a** Thermogravimetric (TGA), **b** differential thermal analysis (DTA), **c** derivative mass loss curves for Al2O3:Cr powder synthesized using a Cr concentration of 10% and different pH values, **d**, **e** curves of TGA and DTA for Al2O3:Cr powder synthesized using a Cr concentration of 1 and 10% and pH 4.0

phase at this pH, almost all the aluminum was in the form of aluminum hydroxide $[Al(OH)_3]$ and was not available for complexation. This demonstrated the importance of complexation of the aluminum ions by NOM, in order to form alpha-alumina. In the case of the sample prepared without NOM and calcined at 1100 °C for 4 h, with initial sol pH 4, the XRD diffractogram indicated no formation of the alpha-alumina phase (Fig. 3b). This confirmed the need for the presence of NOM in order to produce the desired phase.

Figure 3b shows the XRD diffractograms obtained for the non-calcined samples (gels) and the samples produced using different dopant concentrations and calcination temperatures, maintaining an initial pH of 4.0 and a calcination time of 4 h. The diffractograms showed similar profiles for the samples calcined at the same temperature but
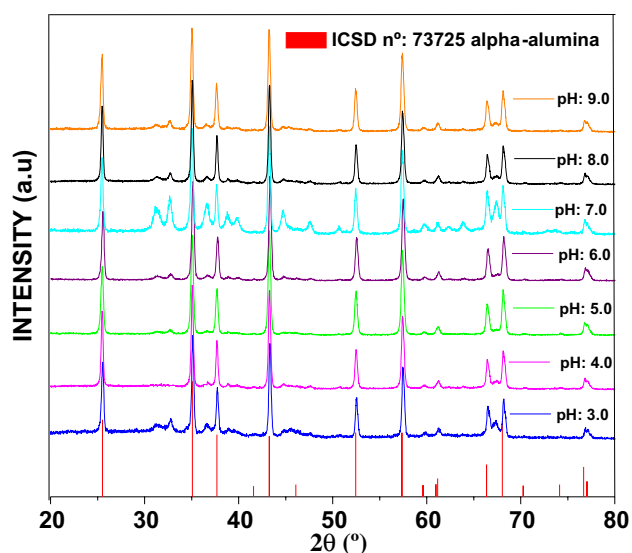
Fig. 2 X-ray diffraction patterns for the Al2O3:Cr (2%) sample prepared using different initial sol pH values. Conditions: Concentration = 0.05 g mL^{-1}; calcination at 1100 °C for 4 h. The ICSD N°. 73725 alpha-alumina standard is included for comparison

with different dopant concentrations. These results were supported by the TGA/DTA curves as well as by previous findings that alteration of the dopant concentration did not affect the diffractogram profile [23, 24, 28]. In addition, the samples showed the presence of the gamma phase and some characteristic peaks corresponding to the alpha phase.

Single-phase alpha-alumina was observed for the sample calcined at 1100 °C (Fig. 4). In previous work concerning the production of non-doped alumina using NOM [20], single-phase alpha-alumina was obtained after crystallization

at 1000 °C for 4 h, so it can be hypothesized that the insertion of Cr ions enhanced the activation energy for crystallization of alpha-alumina. In some cases, this might be due to greater local disorder near the dopant ions [21, 29]. It can also be seen (Fig. 4) that the alpha-alumina phase was obtained for all the dopant concentrations tested, indicating that the temperature for formation of the alpha-alumina phase was not influenced by the dopant concentration, as reported in earlier studies [23, 24, 28].

Figure 4 also shows the XRD patterns for the alumina powder doped with different concentrations of chromium and calcined at 1100 °C for 4 h. All the samples presented well-defined diffraction peaks corresponding to alpha-alumina, indicating a high degree of crystallization. The absence of other diffraction peaks indicated that single phase Al_2O_3 was obtained and that Cr was well incorporated into the host matrix. Since the ionic radius of Cr^{3+} (0.64 Å) is similar to that of Al^{3+} (0.50 Å), no noticeable change in the lattice parameters was expected, even with 10% doping. The positions and widths of the main XRD peaks were the same for all the Cr-doped samples (Fig. 4b), reflecting similar cell parameters and crystallite sizes for all the doped samples. From these results, it could be concluded that the dopant concentration did not affect the crystallization temperature of the alpha-alumina, which remained at 1100 °C (for 4 h) when an initial pH of 4.0 was employed for the precursor colloidal suspension. These findings are indicative of practical advantages for industrial production, because the same synthesis conditions could be used for any dopant concentration.

Analysis using infrared absorption spectrometry enabled evaluation of the vibrational modes of the Al–O bond in octahedral and tetrahedral configurations, as well
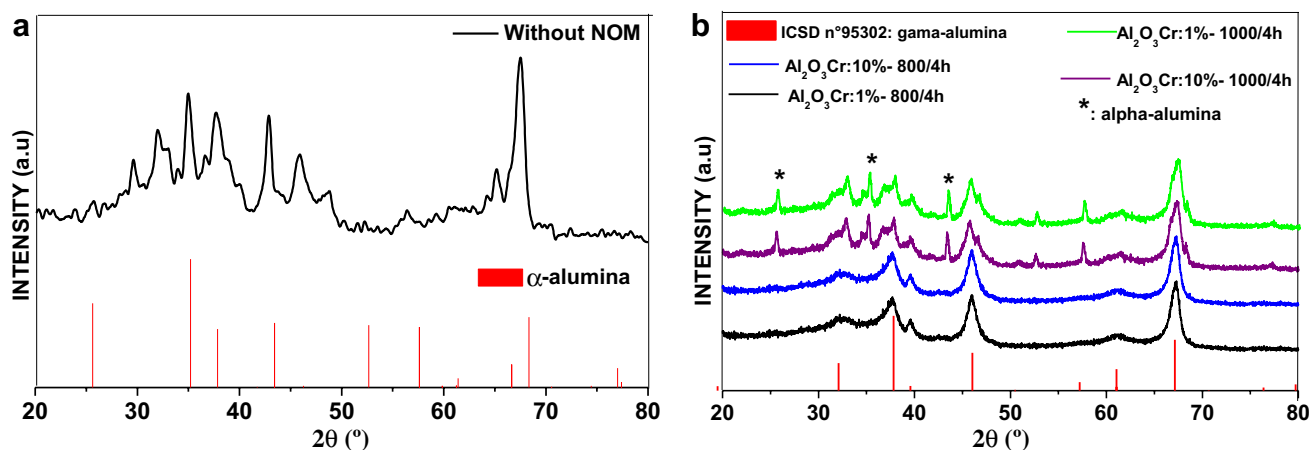

Fig. 3 X-ray diffraction patterns for Al2O3:Cr, **a** sample prepared without NOM and calcination of the powders for 4 h temperature 1100 °C to Al2O3:Cr-1% and **b** calcination of the powders for 4 h at different temperatures to concentration 1 and 10%. Conditions: initial

sol pH 4; concentration = 0.05 g L^{-1}. The diffractogram of the ICSD 95302 gamma-alumina and alpha-alumina (ICSD 73725) standard is included for comparison
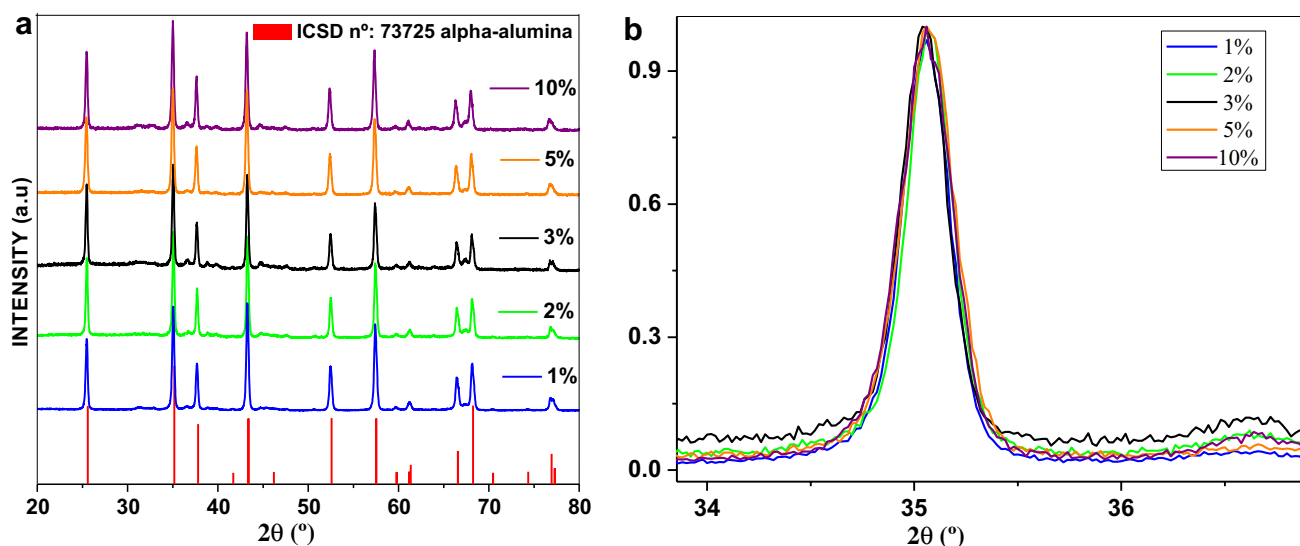
Fig. 4 a X-ray diffractograms for the Al2O3 doped with different concentrations of chromium. Conditions: Concentration = 0.05 g mL^{-1}; initial sol pH 4.0; calcination at 1100 °C for 4 h. The ICSD N°. 73725 alpha-alumina standard is included for comparison and **b** zoom view of the main diffraction peak of doped samples

as the effects of the chromium ions and pH on the alumina vibrational modes. Alpha-alumina shows frequencies of 639, 594, and 447 cm^{-1}, while the frequencies for the tetrahedral coordination (AlO$_4$) are 822, 740, and 530 cm^{-1}. Figure 5 presents the FTIR spectra obtained for alumina doped with different concentrations of chromium ions, showing characteristic bands of alpha-alumina for all the samples. No clear vibrational frequencies were associated with the typical chromium–oxygen sites, so it could be concluded that the presence of this dopant did not significantly affect the characteristic vibrational modes of alpha-alumina.

The initial sol pH can have a significant influence on the vibrational modes of the Al–O bond [30]. It can be seen from Fig. 5b that the vibrational modes associated with the tetrahedral coordination of Al were present for all the samples, with the exception of the sample produced using pH 4.0. Furthermore, octahedral bands were present for all the samples, except those produced using pH 7.0, 8.0, and 9.0.

Table 1 provides the concentrations of impurities in the sample of alumina doped with 10% chromium. It could be concluded that the samples synthesized using NOM-rich water contained low concentrations of the elements Cl, S, Si, Fe, Cu, and Zn. Chlorine was present at
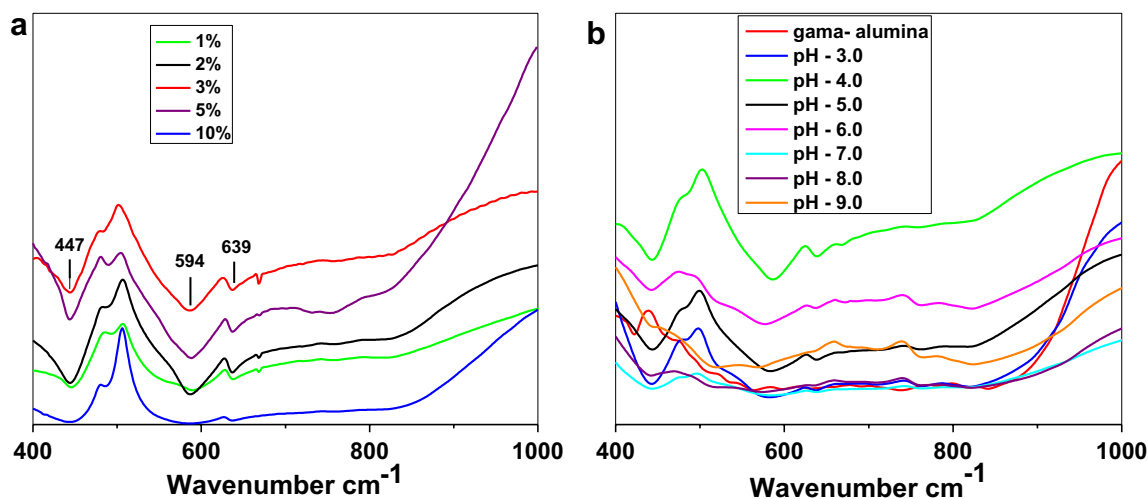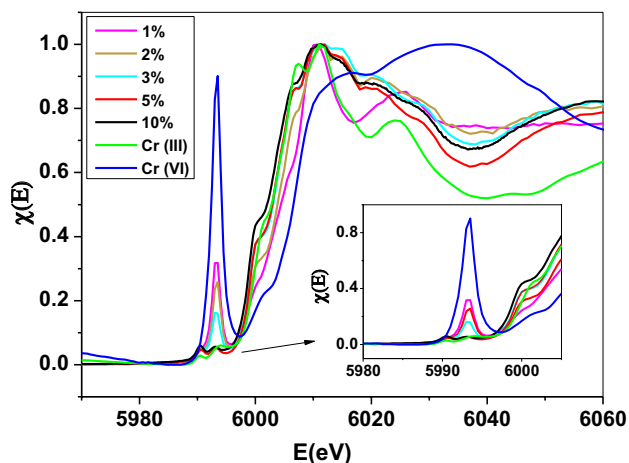

Fig. 5 FTIR spectra of samples produced using **a** different concentrations of dopant, and **b** different pH

Table 1 XRF analysis of impurities in the sample of alumina doped with 10%

Element	Concentration
Al	82.1 ± 1.2
Cr	10.4 ± 0.4
Cl	3.6 ± 0.1
Si	2.1 ± 0.8
S	0.81 ± 0.3
Fe	0.53 ± 0.1
Cu	0.35 ± 0.01
Zn	0.11 ± 0.07

Fig. 6 XANES spectra for alumina powder doped with different concentrations of high purity chromium, and for the Cr_2O_3 (III) and $K_2Cr_2O_7$ (VI) reference materials. Conditions: concentration = 0.05 g mL^{-1}; initial sol pH 4.0; calcination at 1100 °C for 4 h

the highest concentration, which could have been due to the use of aluminum chloride as the reaction precursor, or the water used in the synthesis (because surface waters contain significant amounts of chloride). The element detected at the second highest concentration was silicon, which was possibly derived from soil. The elements S, Fe, Cu, and Zn were detected at significantly lower concentrations.

The XANES spectrum for the Cr(VI) reference material (Fig. 6, blue curve) presented an intense peak in the pre-edge region, which was not found for the Cr(III) reference material (Fig. 6, green curve). Moreover, the absorption edge, determined by the inflection point of the absorption, occurred at higher energies for Cr(VI) (Eo = 6008 eV), compared to Cr(III) (Eo = 6006 eV). The Al_2O_3:Cr(1%), Al_2O_3:Cr(2%), and Al_2O_3:Cr(3%) samples showed the characteristic Cr^{6+} peak In the pre-edge region. However, the Al_2O_3:Cr(5%) and Al_2O_3:Cr(10%) samples did not show this peak, indicating that Cr^{6+} was absent. Due to the toxicity of Cr^{6+}, the presence of this ion in the material is undesirable for industrial applications. The results obtained

here therefore showed that it was possible to produce alumina-doped samples free from this toxic species.

The particle morphology was not influenced by the concentration of Cr employed (Fig. 7) and all the samples presented spherical morphology, with average particle sizes of 41.8 ± 2.1, 40.2 ± 1.1, 42.2 ± 1.6, 39 ± 1.6, and 41.1 ± 1.0 nm for alumina doped with 1, 2, 3, 5, and 10% chromium, respectively. This indicated that the dopant concentration did not influence the particle size and that the modified sol–gel route with NOM was effective in producing nanostructured materials.

Figure 8a shows the emission spectrum of the sample doped with 2% Cr, with emission bands at around 686, 704, and 707 nm. The same emission bands were also observed for the samples prepared using other Cr concentrations. In earlier work, Cr-doped alpha-alumina calcined at temperatures above 1100 °C for 4 h presented the well-known R1 and R2 lines located at approximately 689 and 696 nm, respectively [31]. These bands are related to the position of the chromium ions in the matrix, which causes a distortion [31–33]. The spectrum also showed several less intense bands that resulted from the presence of paired Cr ions in the matrix [31, 32]. Since the PL spectra of the samples produced with NOM were the same as those reported for samples produced by unmodified sol–gel routes, it could be concluded that the use of NOM-rich water to produce the alumina preserved the optical properties of the material.

Figure 8b shows the emission spectra of the samples doped with different Cr concentrations (1–10%). In the case of the samples doped with 1, 2, 3, or 5% Cr, the emission band at 697 nm was in agreement with results reported for samples produced by traditional methods [34–38]. The presence of this peak is due to the $^2E_g \rightarrow {}^4A_{2g}$ transition [36] related to the defects arising from the Cr substitution.

The spectra shown in Fig. 9a revealed that the emission efficiency was influenced by the concentration of Cr ions in the alumina matrix. Similar results have been reported for Cr-doped alumina synthesized using combustion and hydrothermal methods [30, 36]. For low concentrations of dopant, the emission intensity was lower because there were fewer luminescence centers. For higher concentrations, the emission efficiency increased, reaching a maximum for a concentration of 2% and then decreasing for higher concentrations, with complete suppression when a concentration of 10% was used. These findings are consistent with the existence of a cross-relaxation mechanism, which depends on the distance between the dopant ions. Furthermore, for higher concentrations, there is saturation of the host alumina network [32, 34, 37–40].

Figure 9b also presents the excitation spectra for the samples with emissions centered at about 697 nm. Two bands can be observed for the samples doped with 1, 2, 3, and 5% of chromium, with maxima at 400 and 550 nm,

Fig. 7 SEM images of chromium-doped alumina powders produced by the NOM assisted sol–gel route using different Cr concentrations: **a** 1%, **b** 2%, **c** 3%, **d** 5%, and **e** 10%. Conditions: initial sol pH 4.0; stirring time = 30 min; calcination at 1100 °C for 4 h
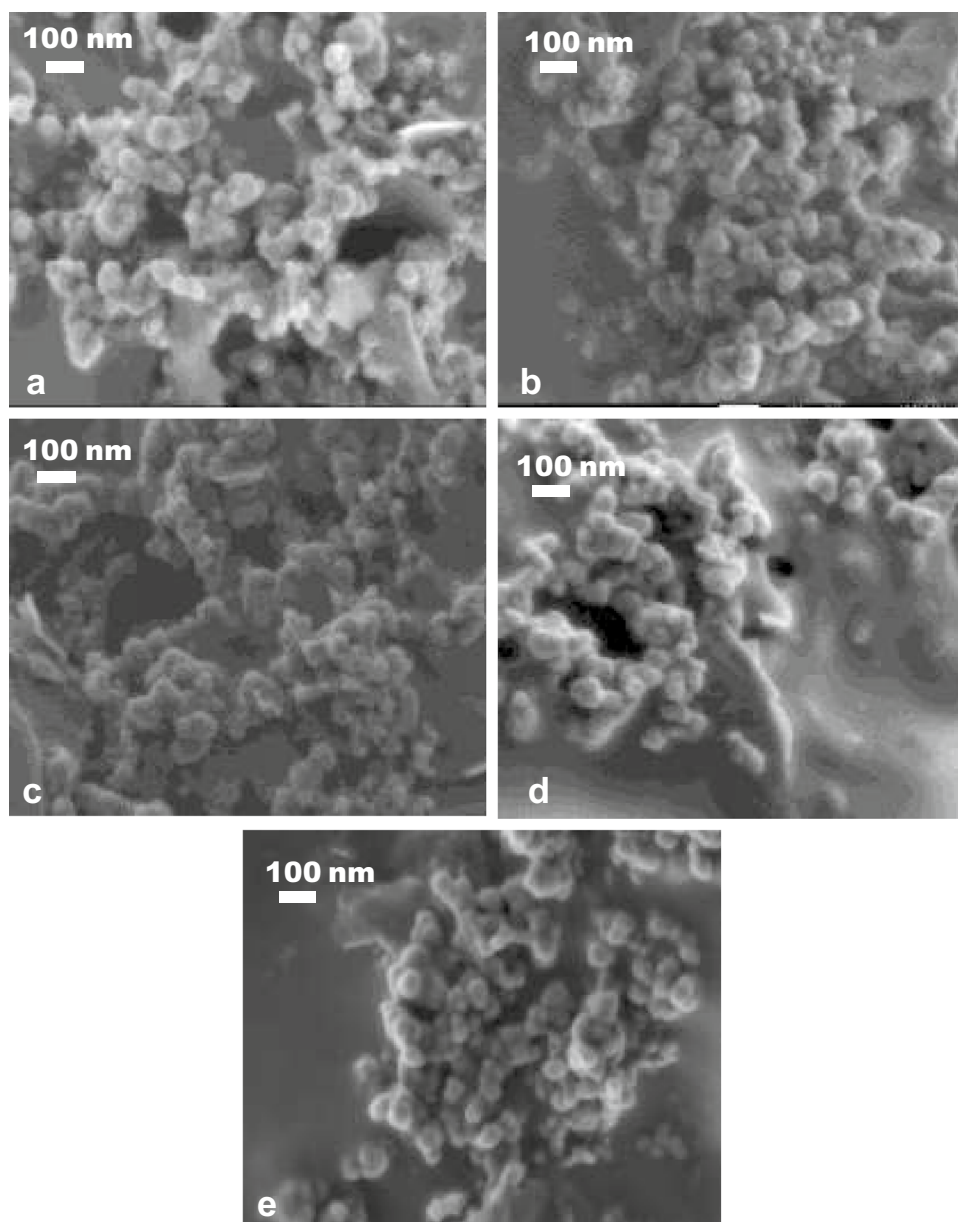
related to Cr transitions $^4A_{2g} \rightarrow {}^4T_{1g}$ and $^4A_{2g} \rightarrow {}^4T_{2g}$, respectively [39, 40]. It can be seen that the intensities of these bands were dependent on the dopant concentration. Although NOM-rich water may contain several impurities, the effect of these impurities did not seem to influence the optical properties of the samples tested in this work.

Figure 8b compares the light outputs measured for the non-doped and 2% Cr-doped samples. It could be concluded that the emission was due to the presence of Cr in the sample, since the non-doped alumina did not show any light emission.

Figure 9 presents the XEOL curves obtained for the samples doped with different concentrations of chromium (1–10%). The spectra showed that the emission efficiency was influenced by the concentration of chromium ions in the alumina matrix, with lower emission intensity at low chromium concentrations. The emission intensity reached a maximum at a chromium concentration of 2%, with decreased radioluminescence efficiency at higher concentrations. Radioluminescence was suppressed at a concentration of 10%. All the spectra showed the same behavior as the PL curves.

Figure 10 presents the chromaticity diagram for the alumina doped with different concentrations of high purity chromium (1–10%), using different initial sol pH values (pH 3.0–9.0). The intensity of the pink color increased in line with the concentration of the dopant, so different tones
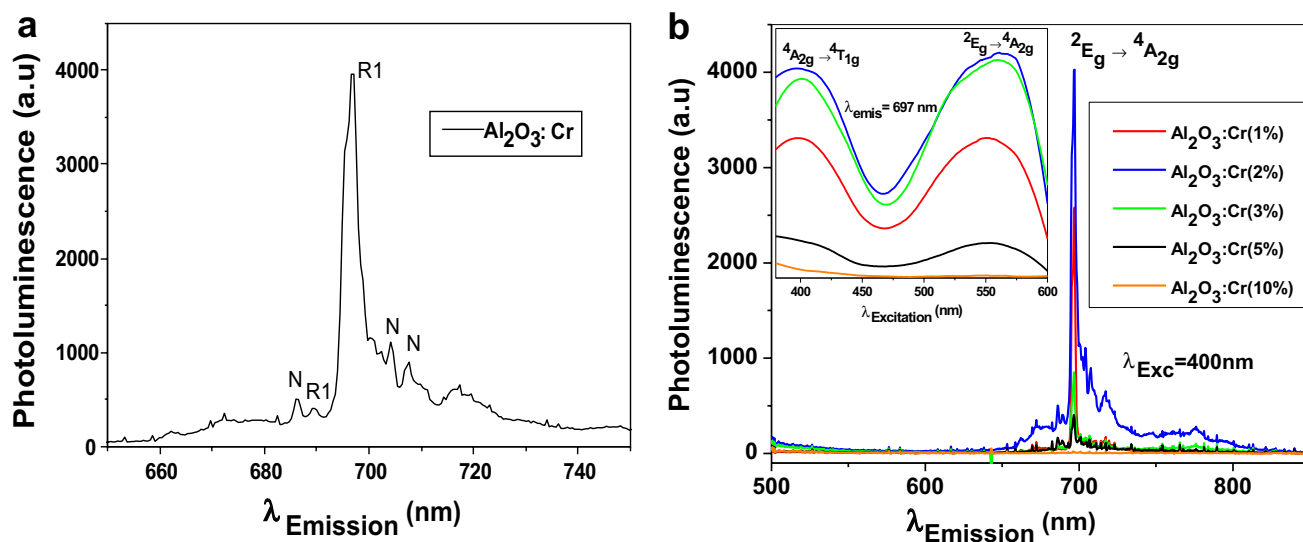
Fig. 8 a Emission spectrum of the alumina doped with 2% chromium, synthesized using NOM-rich water and **b** Excitation and emission spectra for alumina doped with different concentrations of chromium. Conditions: initial sol pH 4.0; calcination at 1100 °C for 4 h
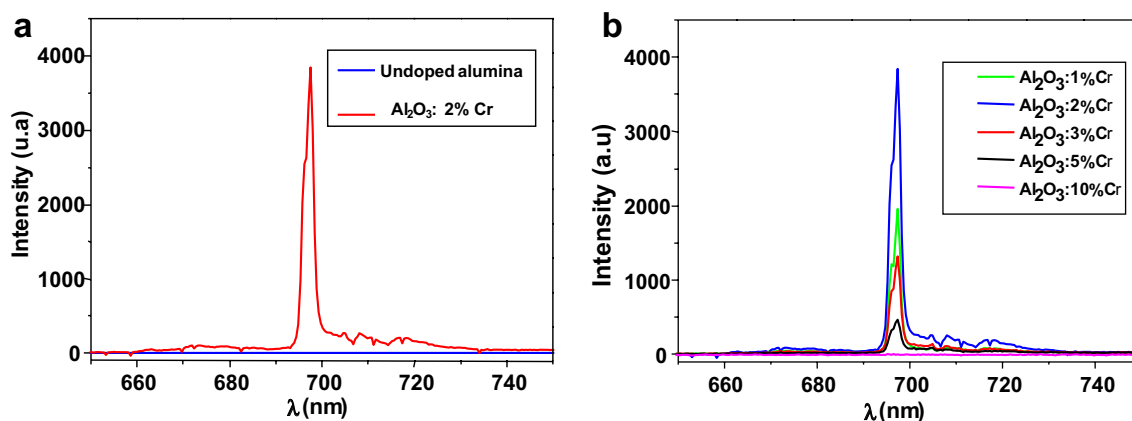

Fig. 9 a XEOL emission spectra of the non-doped and 2% chromium-doped alumina samples and XEOL emission spectra of the alumina doped with different concentrations of chromium. Conditions:

E = 8 keV; initial sol pH 4.0; calcination at 1100 °C for 4 h (doped); concentration = 0.05 g mL^{-1}

were obtained by only varying the dopant concentration. This significantly affected the chromaticity coordinates of the doped alumina. For example, the sample obtained using an initial sol pH of 3.0 (indicated in the diagram with the letter "f") presented a significantly less intense pink tone, compared to the sample synthesized using the same concentration of dopant, but at pH 4.0, indicated in the diagram with the letter "b". These results were possibly due to the different mixtures of phases present, which depended on the pH (Fig. 4).

Leaching tests were performed according to the NBR-10005 protocol. No significant concentrations of total chromium (determined by ICP-OES) were detected in any of the tests. Therefore, the use of NOM-rich water for the

synthesis of nanopigments composed of alumina doped with chromium would not harm the environment.

4 Conclusions

Synthesis of chromium-doped alpha-alumina nanopowder using water rich in aquatic humic substances is both eco-friendly and highly practical. The best synthesis conditions for obtaining a single-phase nanostructure using this green biological route were pH 4.0 and calcination at 1100 °C for 4 h. The results of XRD and FTIR analyses confirmed formation of the alpha-Al$_2$O$_3$:Cr phase. The chromaticity data revealed that the pink color intensified
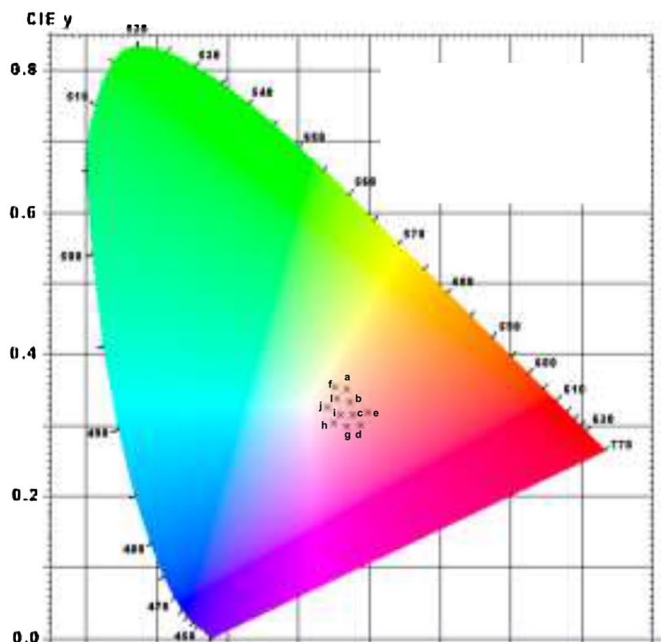
Fig. 10 Chromaticity diagram of the alumina samples doped with different concentrations of chromium (*a*: 1%; *b*: 2%; *c*: 3%; *d*: 5%; *e*: 10%) and initial sol pH 4.0, diagram of the alumina samples doped with 2% of chromiun and using different initial sol pH values (*f*: 3.0; *g*: 4.0; *h*: 5.0; *i*: 7.0; *j*: 8.0; *l*: 9.0)

with increasing dopant concentration. The SEM results indicated that the particles obtained in the present work were spherical and smaller than 42 nm. The luminescence and radioluminescence spectra of the nanoparticles were sensitive to the dopant concentration, and the spectra were identical to the profiles described in the literature for samples synthesized using traditional routes, which supports the technological feasibility of the proposed synthesis route. This new methodology could be employed for the production of phosphorescent nanomaterials used in the development of various sensors and new types of polycrystalline ceramic lasers, since the impurities present in the NOM-rich water did not affect the optical properties of the alpha-alumina doped with chromium.

References

1. N.L. Tarwal, P.R. Jadhav, S.A. Vanalakar, S.S. Kalagi, R.C. Pawar, J.S. Shaikh, S.S. Mali, D.S. Dalavi, P.S. Shinde, P.S. Patil, Powder Technol. **208** (2011)
2. A.V. Dijken, E.A. Meulenkamp, D. Vanmaekelbergh, J. Lumin. **90** (2000)
3. F. Chouli, I. Radja, E. Morallon, A. Benyoucef, Synth. Charact. Electrochem. Prop. (2015). doi:10.1002/pc.23837.
4. S. Benykhlef, A. Bekhoukh, R. Berenguer, A. Benyoucef, E. Morallon, Synth. Charact. Electrochem. Stud. **294** (2016)
5. P. Kathirvel, J. Chandrasekaran, D. Manoharan, J. Alloys Compd. **590** (2014)
6. B. Huang, C.H. Bartholomew, B.F. Woodfield, Microporous Mesoporous Mater. **183** (2014)
7. X. Fu, W. Tang, L. Ji, C. Shifu, Chem. Eng. J. **180** (2012)
8. N. Mandlik, P.D. Sahare, M.S. Kulkarni, B.C. Bhatt, V.N. Bhoraskar, S.D. Dhole, J. Lumin. **146** (2014)
9. M.P. Chougaonkar, B.C. Bhatt, Radiat. Prot. Dosimetry 112 (2004)
10. J.S. Lee, H.S. Kin, N. Park, Chem. Eng. J. **230** (2013)

11. P.B.R. Gasparian, F. Vanhavere, E.G. Yukihara, Radiat. Meas. **47** (2012)
12. N.S. Wang, M. Shao, G. Shao, Chem. Phys. Lett. **460** (2008)
13. X. Mi, X. Zhang, X. Ba, Adv. Powder Technol. **20** (2009)
14. N. Salah, H.Z. Khan, S.S. Habib, Nuclear Instrum. Methods Phys. Res. Sect. B. **269** (2009)
15. Y. Marinova, J.M. Hohemberger, E. Cordoncillo, P. Escribano, J.B. Carda, J. Eur. Ceram. Soc. **23** (2003)
16. G.K. Naika, P.M. Mishra, K. Parida, Chem. Eng. J. **229** (2013)
17. M. Faramarzi, A. Sadighi, Adv. Colloid Interface Sci. **189** (2013)
18. M. Nidhin, K.J. Sreeram, B. Nair, Chem. Eng. J. **185** (2012)
19. H. Liu, J. Huang, D. Sun, Chem. Eng. J. **209** (2012)
20. G. da C. Cunha, L.P.C Romão, Z.S. Macedo, Powder Technol. **254** (2014)
21. A.M. Gomes, M.E.G. Valerio, J.F.R. Queiruga, Z.S. Macedo, Mater. Chem. Phys. **142** (2013)
22. J. Li, Y.B. Pan, C.S. Xiang, Ceram. Intl. **32** (2006)
23. I. Radja, H. Djelad, E. Morallon, A. Benyoucef, Synth. Met. **202** (2015)
24. H.S. Hafez, E. El-fadaly, Spectrochim. Acta Part A Mol. Biomol. Spectrosc. **95** (2012)
25. S. Sivakumar, A. Venkatesan, P. Soundhirarajan, P.C. Khatiwada. Spectrochim. Acta Part A Mol. Biomol. Spectrosc. **151** (2015)
26. K.H. Tan, *Principles of Soil Chemistry*, 2nd edn. (CRC Press, New York, 2014), pp. 46–52
27. M.A. Gomes, M.E.G. Valerio, Z.S. Macedo, J. Nanomaterials **2011** (2011)
28. C. Mayrinck, D.P. Santos, S.J.L. Ribeiro, M.A. Schiavon, J.L. Ferrari, Ceram. Intl. **40** (2014)
29. M.T. Hernández, M. González, J. Eur. Ceram. Soc. **22** (2002)
30. G. Rani, P.D. Sahare, Adv. Powder Technol. **25**, 767–772 (2014)
31. A. Patra, R.E. Tallman, B.A. Weinstein, Optic. Mater. **27** (2005)
32. A. Zuo, P.W. Jagodzinski, Appl. Spectrosc. **56** (2002)
33. A.B. Kulinkin, S.P. Feofilov, R.I. Zakharchenya, Phys. Solid State **42** (2000).
34. C. Zhu, S. Hosokai, T. Akiyama, J. Hydrogen Energy **37** (2012)
35. Q. Liu, Q.H. Yang, G.G. Zhao, J. Alloys Compd. **579** (2013)
36. F. Liu, J. Huang, J. Jiang, J. Eur. Ceram. Soc. **33** (2013)
37. Q. Liu, Q. Yang, G. Zhao, S. Lu, J. Alloys Compd. **582** (2014)
38. T. Cheng, H.E. Allen, J. Environ. Manage. **80** (2006)
39. C. Pan, S. Chen, P. Shen, J. Cryst. Growth **310** (2014)
40. K. Fujita, Y. Tokudome, K. Nakanishi, J. Non-cryst. Solids **354** (2008)